Proc. Natl. Acad. Sci. USA
Vol. 90, pp. 3127–3133, April 1993

Review

Nuclear magnetic resonance imaging and spectroscopy of human brain function

R. G. Shulman†, A. M. Blamire†, D. L. Rothman‡, and G. McCarthy§¶

Departments of †Molecular Biophysics and Biochemistry, ‡Internal Medicine, and ¶Neurosurgery, Yale University, New Haven, CT 06510; and §Veterans Administration Medical Center, West Haven, CT 06516

ABSTRACT **The techniques of *in vivo* magnetic resonance (MR) imaging and spectroscopy have been established over the past two decades. Recent applications of these methods to study human brain function have become a rapidly growing area of research. The development of methods using standard MR contrast agents within the cerebral vasculature has allowed measurements of regional cerebral blood volume (rCBV), which are activity dependent. Subsequent investigations linked the MR relaxation properties of brain tissue to blood oxygenation levels which are also modulated by consumption and blood flow (rCBF). These methods have allowed mapping of brain activity in human visual and motor cortex as well as in areas of the frontal lobe involved in language. The methods have high enough spatial and temporal sensitivity to be used in individual subjects. MR spectroscopy of proton and carbon-13 nuclei has been used to measure rates of glucose transport and metabolism in the human brain. The steady-state measurements of brain glucose concentrations can be used to monitor the glycolytic flux, whereas subsequent glucose metabolism—i.e., the flux into the cerebral glutamate pool—can be used to measure tricarboxylic acid cycle flux. Under visual stimulation the concentration of lactate in the visual cortex has been shown to increase by MR spectroscopy. This increase is compatible with an increase of anaerobic glycolysis under these conditions as earlier proposed from positron emission tomography studies. It is shown how MR spectroscopy can extend this understanding of brain metabolism.**

During the last century it has become evident that sensory, motor, and cognitive functions can be mapped to discrete anatomical regions of the human brain. Early functional localization was often based upon changes in function following discrete brain lesions. These studies were extended by experiments in which electrical stimulation of discrete brain regions elicited movements, sensations, or complex cognitive functions such as language comprehension or memory. Powerful methods of modern biology have increasingly been concentrated on understanding brain function. Pioneering work of Kety and Schmidt (1) stimulated research on the coupling between brain electrical activity, metabolism, and cerebral blood flow. Recent radiolabel measurements, particularly positron emission tomography (PET) of spatially localized blood flow and metabolism, have provided new insights into the mapping of brain activity (2). The visual cortex has been the subject of particularly intense physiological, pharmacological, histological, and functional studies, although other sensory regions have been actively explored (3). Even complex cognitive functions of the frontal cortex are being identified and localized (4–6).

In the past few years nuclear magnetic resonance (NMR) spectroscopy (MRS) and NMR imaging (MRI) have been used to map brain function. Both methods take advantage of the spin magnetic moment of certain nuclei, which usually have been ^1H, ^{13}C, or ^{31}P. When placed in a static magnetic field (B_0), the nuclear magnetic moment results in the nuclear spin projections being quantized with respect to the magnetic field. The energy difference between parallel and antiparallel orientations in frequency units is proportional to the magnetic field by the Larmor relation $\nu = (\gamma/2\pi)B_0$, where γ is the gyromagnetic ratio characteristic of the particular nucleus. In the NMR experiment, transitions between spin orientations are induced by a radio frequency (RF) field at the Larmor frequency. The RF signal emitted by the NMR transition is measured by magnetic induction in a receiver coil. The B_0 fields available for human brain experiments limit the Larmor frequency to the 20- to 200-MHz range. MRI measures the spatial distribution of magnetic nuclei by using magnetic "gradient" coils to produce a linear dependence of the B_0 field on position, thereby establishing a direct connection between Larmor frequency and location. During acquisition of the MRI signal, the gradient coils are pulsed on three orthogonal axes to spatially encode the signal. After the signal is stored in a computer, a multidimensional Fourier transformation is applied to produce an image of the spatial distribution of the water signal. The image is divided into equal-size volume elements, which are called "voxels." The difference in signal intensity between different voxels creates an image with contrast. Because of the high concentration of H_2O *in vivo* (≈40 M), the NMR signals are strong, so that modern MRI systems can resolve structures as small as 1 mm^3 in humans. Imaging has been rapidly developed since 1973 (7), so that by 1977 images of H_2O in the human body had been reported (8) and by 1983 commercial instruments were being installed in hospitals for clinical service.

MRS *in vivo* builds upon well-established methods, which show that the same nucleus—i.e., ^1H, ^{13}C, or ^{31}P—at different molecular sites will resonate at different frequencies in the same B_0 field, thereby allowing resonances in the spectrum to be resolved and assigned to specific sites in different molecules. The first *in vivo* NMR spectra were obtained of the ^{31}P nuclei in a suspension of erythrocytes (9). MRS studies of humans, which began with ^{31}P NMR of limbs (10), have been extended to include ^{13}C and ^1H NMR observations (11) and are now routinely made on the human abdomen and brain.

It is the purpose of this article to show how recent developments of MRS and MRI methods for studying the human brain are beginning to provide information about the spatial localization and metabolic changes associated with human brain activity. We sketch, at this early stage, the nature of these new NMR methods and indicate their accomplishments and promise as well as their present availability and limitations.

MRI Studies of Brain Functional Activation

Physical Dependencies of the MRI Signal. In MRI measurements of function-

Abbreviations: NMR, nuclear magnetic resonance; MRS, magnetic resonance spectroscopy; MRI, magnetic resonance imaging; PET, positron emission tomography; rCBF, regional cerebral blood flow; rCBV, regional cerebral blood volume; $rCMR_{glc}$, regional cerebral metabolic rate of glucose; $rCMRO_2$, regional cerebral metabolic rate of oxygen; T_1, longitudinal (spin-lattice) relaxation time; T_2, transverse (spin-spin) relaxation time; T_2^*, apparent T_2; TE, echo time; ν_{tca}, tricarboxylic acid cycle rate; FLASH, fast low-angle shot method; EPI, echo–planar imaging.

related changes in brain activity (functional MRI), the activated regions are mapped on the basis of changes in regional cerebral blood flow (rCBF), volume (rCBV), or oxygen metabolic rate ($rCMRO_2$), which affect the NMR relaxation times T_2^* or T_1. In the MRI experiment, RF excitation of the H_2O proton spins (which induce the NMR signal) also drives the spins from thermal equilibrium. The time required for the system to return to thermal equilibrium is characterized by a decay constant T_1 known as the longitudinal (spin–lattice) relaxation time. The rate of the return to equilibrium is increased if nonexcited spins enter the region, so that T_1 measurements of H_2O are affected by tissue perfusion. After excitation, the NMR signal decays exponentially with a decay constant T_2 known as the transverse (spin–spin) relaxation time. If the applied B_0 field is inhomogeneous and varies spatially across the voxel, the signals from different portions of the voxel lose phase coherence, resulting in a shorter decay constant, the apparent T_2 designated T_2^*. These inhomogeneities arise from two sources: (*i*) the macroscopic (m) inhomogeneities due to imperfections in the magnet and inhomogeneities produced at interfaces between the brain and large regions of different magnetic susceptibility, such as the air-filled sinuses; and (*ii*) microscopic (μ) variations in susceptibility of which erythrocytes in the capillaries are the major biological contributor but which can be enhanced by intravascular injection of paramagnetic complexes called contrast agents. The result of these field variations on T_2^* can be expressed as

$$1/T_2^* = 1/T_2 + 1/T_2^m + 1/T_2^\mu, \quad [1]$$

where $1/T_2^m$ and $1/T_2^\mu$ are the additional signal decay rates due to B_0 inhomogeneity. The magnitudes of these field variations are proportional to B_0, making T_2^* shorter at higher magnetic fields.

The majority of functional MRI experiments have measured changes in T_2^* induced by brain activity. These changes are measured by subtracting images obtained in a baseline state from those acquired during activation, voxel by voxel. They arise from changes in the microscopic magnetic environment around the capillaries that alter T_2^μ and consequently T_2^* (Eq. 1). For the voxel intensity to be sensitive to T_2^*, a time delay referred to as echo time (TE) is placed between RF excitation and image acquisition during which the signal (S) in each voxel decays by

$$S(TE) = S(0)\exp(-TE/T_2^*). \quad [2]$$

Since T_2 and T_2^m are not expected to change during brain activation, the fractional change in image intensity depends only on T_2^μ and TE. With a refocusing pulse sequence, the signal intensity depends upon TE and T_2 instead of T_2^*, and this sequence is sometimes useful in functional imaging.

Fast MRI Methods. Functional images can be obtained at subsecond resolution by using fast MRI methods. In addition to allowing short-lived brain processes to be studied, fast MRI has the advantage of obtaining images undistorted by sample motion. There are two main types of fast MRI: (*i*) methods that require multiple RF excitations such as the FLASH (fast low-angle shot; ref. 12) method and (*ii*) echo–planar imaging methods (EPI) (13), which require a single RF excitation. Multiple excitation methods require at least one RF pulse for each line of the image matrix (12, 14). In the FLASH method, each line is acquired in ≈5–15 ms, giving a total acquisition time of 1.5–4 s for a 256 × 256 image matrix. Smaller image matrices require proportionally less time, since fewer lines are sampled. To minimize the acquisition time, it is necessary to apply excitation pulses close together, and extensions of the FLASH method such as Turbo-FLASH can reduce the data collection time to ≈300 ms (15). The EPI technique uses a single excitation pulse acting on the full equilibrium magnetization and then collects the full image data in a single acquisition. Typical total acquisition times for EPI are 40–128 ms, which are capable of eliminating almost all effects of subject motion during acquisition. However, for all MRI methods, motion between images can complicate interpretation of changes in voxel intensity, and some form of head restraint is desirable. The EPI experiment requires high-field homogeneity (long values of T_2^m), as the magnetic coherence must last longer than during multiple RF methods. In addition, EPI acquisition requires more rapid switching of the B_0 gradients than do the FLASH methods, and this switching is generally not available on clinical MRI instruments.

MRI Studies of Functional Brain Activation Using Contrast Agents. In pioneering experiments at the Massachusetts General Hospital, it was shown that a bolus of the standard MRI contrast agent, a chelate complex between diethylenetriaminepentaacetic acid (DTPA) gadolinium(III) (Gd–DTPA), could be used as a tracer for blood volume (16). Although the Gd–DTPA complex is confined to the vasculature by the blood–brain barrier, the large microscopic magnetic field gradients induced in the capillaries by the paramagnetic gadolinium(III) ion extend into the tissue and drastically reduce T_2^μ and hence T_2^* (Eq. 1). Gadolinium(III) also reduces T_2, presumably by H_2O diffusion into capillaries, which as shown in Eq. 1 will also reduce T_2^*. When an imaging sequence sensitive to T_2^* or T_2 is used, a loss of signal intensity is observed in the image voxels where Gd–DTPA is present. Research with animal models has established an empirical relationship between blood volume and the loss of voxel intensity in a T_2^*- or T_2-weighted MR image as a function of Gd–DTPA concentration (17–19). Belliveau *et al.* (16) exploited this property to study brain function by rapidly injecting a bolus of Gd–DTPA into a vein, where it would pass into the heart and become entirely mixed with all blood destined for the brain. Such a bolus has a transit time of ≈15 s between injection and arrival in the brain, and its effects remain visible for an additional period of ≈15 s. In this experiment a T_2-sensitive EPI imaging sequence (TE = 100 msec) was used to monitor the passage of the bolus through slices of the brain over time. The regional signal changes were converted to a concentration–time curve from which rCBV was calculated. To study brain function, the experiment was performed during a resting state and then again during visual stimulation. By taking the difference between the two CBV maps, an increase in blood volume was demonstrated in the primary visual cortex (Fig. 1) during visual stimulation.

MRI Studies of Brain Activation Using Hemoglobin-Based Contrast. The Gd–DTPA method has the disadvantage of requiring a bolus tracer injection, which has a delay due to delivery and which limits the number of measurements on a subject. In 1990 Ogawa *et al.* (20) demonstrated that an MRI sequence that is sensitized to small changes in T_2^* can detect changes in blood oxygenation level via the local microscopic field gradients created by deoxyhemoglobin (Hb), which is paramagnetic, in contrast to oxyhemoglobin (HbO_2), which is diamagnetic. Changes in the amount of Hb in the capillaries create effects similar to Gd–DTPA but on a much smaller scale. By reducing the level of blood oxygen to increase Hb content while imaging a rat brain at 7 T (tesla), they observed a darkening of the image around the major blood vessels. Further experiments by Ogawa *et al.* (21) using graded levels of anesthesia showed changes in image intensity as the brain activity was reduced that correlated with electroencephalographic recording. In 1991 Turner *et al.* (22) performed similar experiments in cat brain at 2.0 T. Using a T_2^*-sensitive EPI sequence, they subjected the animal to 60 s of N_2 anoxia and observed regional decreases in image intensity as the concentration of Hb in the blood increased. On restoration of the oxygen supply, the signal returned to nearly normal intensity. This demonstrated that transient changes in blood oxygenation could be followed dynamically by using fast MRI.

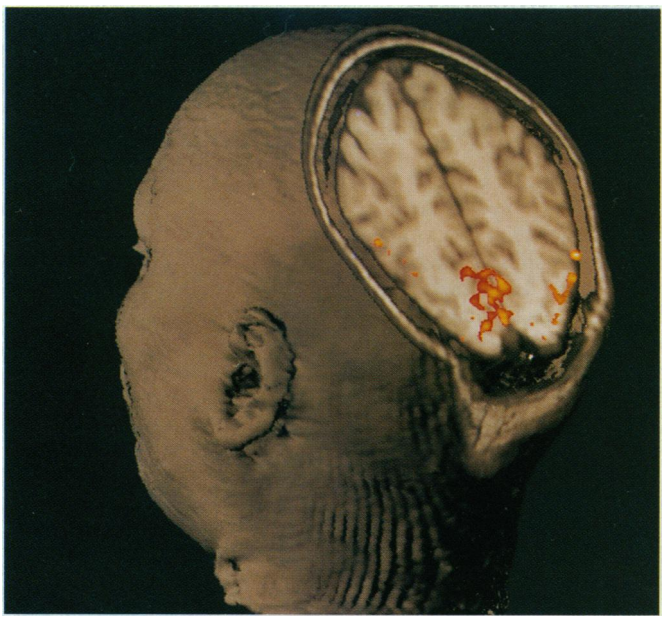

FIG. 1. Color pattern on the human visual cortex reflects a local blood volume change during photic activation. Injected material causes magnetic susceptibility changes as it flows through brain vessels. {Courtesy of J. Belliveau and B. Rosen, Massachusetts General Hospital; reproduced with permission [*Science* (1991) **254,** 621; (copyright AAAS)].}

Several groups have recently applied this method to the study of human brain activation during stimulation of the visual and motor areas of the cortex. Bandettini *et al.* (23) used the EPI sequence with TE = 50 ms at 1.5 T while carrying out a finger-movement task. They observed a 4.3 ± 0.3% increase in signal intensity in localized regions corresponding to the motor cortex. Kwong *et al.* (24) applied the technique to the visual cortex during alternate periods of darkness and full-field visual stimulation. They also used the EPI sequence at 1.5 T with TE = 40 ms and observed a 1.8 ± 0.8% increase in signal. Ogawa *et al.* (25) used a similar visual stimulation paradigm and a fast gradient-echo sequence (TE = 40 ms and total acquisition time = 5–10 s) on a human 4.0-T size MR system. Because of the larger signal changes at the higher field strength (8.2 ± 3.3%), they were able to reduce voxel size to less than the thickness of the cortex, demonstrating that the increase in signal is confined to the gray matter (Fig. 2).

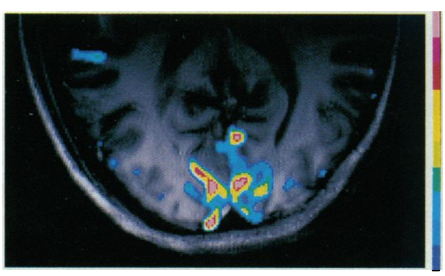

FIG. 2. Visual activation can be detected by NMR without injected material as a result of changes in paramagnetic Hb concentration from oxygen changes during photic stimulation. (Courtesy of K. Ugurbil, University of Minnesota.)

In several studies the temporal response of the image changes to visual stimulation have been measured. Kwong *et al.* (24) applied visual stimulation for 60 s and reported a 4.4 ± 2.2-s delay before the response was detected. Blamire *et al.* (26) measured visual stimulation with EPI at 2.1 T with TE = 70 ms, which gave a 9.7 ± 2.8% change in signal. For a 20-s stimulation period, they measured a mean delay of 5 ± 2 s (n = 20) before a signal change was observed. For a 2-s stimulation period, a response was measured after the stimulation ceased (delay = 3.5 ± 0.5 s). A similar delay has been noted during a motor stimulation task (27). The delayed response presently determines the temporal resolution in this kind of experiment.

MRI studies of functional brain activation depending upon Hb-based contrast have all observed an increase in signal during activation, which suggests that the local (microscopic) field gradients have been reduced. The reduced local field gradients imply a decrease in the amount of Hb in the capillaries, which is seemingly paradoxical considering the increase in $rCMRO_2$ and rCBV associated with neuronal activity. However, it is known from PET studies that regional blood flow also increases during visual stimulation (28), and this may overwhelm the small reported increases in $CMRO_2$. Alternative mechanisms postulating changes in capillary distribution due to recruitment with increased blood flow must also be considered in any complete model of this mechanism.

Since the publication of the first functional MRI results, many groups have repeated the visual-stimulation paradigms (29–31) and extended their experiments to investigate other types of sensory and cognitive stimulation (32, 33, 82). Importantly, it has been shown that conventional imaging methods with data acquisition times of 5–60 s can under the right conditions show the stimulation effects (30, 34, 35). W. Schneider (personal communication) has begun a detailed analysis of the human visual cortex. By using an optical projection system, computer-generated stimulation patterns have been used to excite the different areas of the cortex. Belliveau *et al.* (36) have mapped the increase of signal response to different frequencies of stimulation. Activity in the visual cortex has also been reported during imagined visual stimuli (37). Studies have been made to determine the optimum TE and slice thickness for the imaging experiments (38–40).

We have made echo–planar functional images of word repetition and generation paradigms adapted from PET studies and have observed activation of the left frontal cortex (41) similar to the PET results but with improved temporal and spatial resolution (Fig. 3). A study of the response to passive word presentation has also been made (42).

MRI Studies of Functional Activity-Related Changes in Flow/Perfusion. MRI methods of measuring perfusion are based on Kety's method (43) for measuring cerebral blood flow with a freely

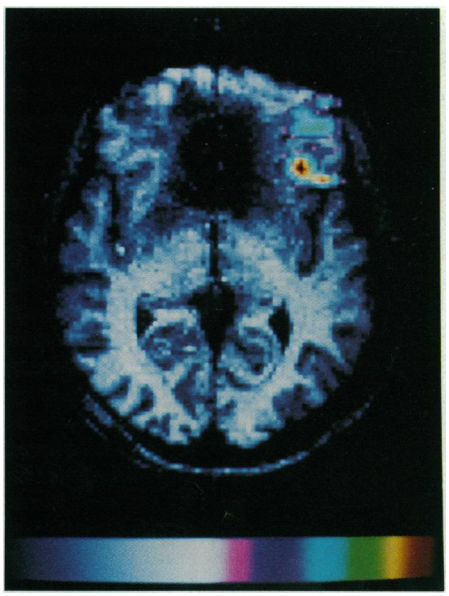

FIG. 3. Functional MR image showing activation of left prefrontal cortex during a verb generation task. Images were acquired during a resting state and while the subject was generating verbs to match auditorily presented nouns. The image shows the increased activity in the left prefrontal cortex (Brodmann's areas 47 and 10) (unpublished data).

diffusible tracer. Adaptations of this principle for MR experiments have used either ^2H_2O (44–47) or $H_2^{17}O$ (48, 49) as exogenous tracers. In other experiments selective inversion of the proton spins by RF excitation labels the endogenous water in the region (24, 50, 51). Under conditions of no blood flow, the observed T_1 is equal to the actual T_1, whereas under conditions with blood flow, H_2O proton spins at thermal equilibrium from outside the region of RF excitation are brought into the system, which hastens the return to equilibrium and allows rCBF to be calculated. It has been demonstrated at 1.5 T with a selective inversion MRI method that blood flow changes can be observed during activation of human visual cortex (24).

Hardware Requirements for Functional MRI. The majority of reported functional imaging studies have been performed at static field strengths available in commercial MR imaging systems—i.e., 1.5–2.0 T. For Hb-contrast MRI, the fractional signal change appears to increase with field strength (81) as expected. At present, systems up to 4 T are in operation, and several have reported functional MRI results (25, 29, 38). The RF requirements for functional MRI are the same as for conventional MRI, although specialized RF coils are required at field strengths above 2 T. To switch the gradients rapidly for subsecond fast imaging it is necessary to have shielded gradient coils, which are presently available on many conventional imaging systems. High-resolution (voxel size $<3 \times 3 \times 10$ mm) EPI requires more powerful gradient amplifiers than are available on most conventional imaging systems or the use of a specialized high-efficiency gradient insert coil (23), which has a smaller diameter than the gradients in conventional imaging systems. Both high-power gradient amplifiers specialized for fast MRI and insert gradient coils are commercially available. To maximize the signal strength during Hb-contrast functional MRI, it is necessary to minimize macroscopic field inhomogeneity by using a set of magnetic shim coils (and hence to maximize T_2^* in Eq. 1). Most commercial systems have adequate shim coils for this purpose, and automated computer routines to perform this minimization process are now available (52) but are difficult to install on clinical systems.

After the MRI signal is digitally sampled, it is stored in computer memory. A typical fast MRI requires 16 kilobytes of data per slice (128×128 matrix), and since multiple slice images are obtained every few seconds, the data storage requirements are severe. Fourier transformation and subsequent numerical analysis and three-dimensional display of large image data sets demand high computer speed and graphics capabilities, and systems are presently being developed that are optimized for this purpose.

MRS Studies of Functional Activity and Metabolism

MRS studies of functional activity-related changes in brain metabolism depend mainly upon the ^1H nucleus, which is the most NMR-sensitive to maximize signal strengths of the dilute metabolites that are in the millimolar range. ^1H MRS measurements of metabolites require voxels of >1 cm^3 and acquisition times of several minutes. Initial studies on animal brain (53, 54) demonstrated that several resonances of compounds relevant to metabolic studies can be measured including alanine, aspartate, glutamate, glutamine, γ-aminobutyric acid, and lactate. Initial human studies (55, 56) were limited to the strongest resonances in the ^1H NMR spectrum, which are from *N*-acetylaspartate, from creatine and phosphocreatine, and from quaternary ammonium methyl groups—e.g., choline. Only recently with improvements in MRS methodology have adequate sensitivity and resolution been obtained to study the weaker resonances of lactate, glutamate, and glucose in humans. Some of the potential uses of the resonances for studying metabolism and recent applications to studies of metabolic changes during visual stimulation are described below.

MRS Methods for Measuring Anaerobic Glycolysis. The basal concentration of lactate in the human brain was measured by ^1H MRS homonuclear editing techniques to be $\approx$0.6 mM (57). Earlier animal studies had shown that ^1H MRS can measure elevation of lactate due to anaerobic glycolysis during hypoxia, anoxia, and ischemia (53). ^1H MRS measurements of lactate intensity have been made in tumor and stroke, where its concentration has been followed over time and its spatial distribution plotted (58–60). In addition to measuring lactate concentration, ^1H MRS has been used to follow lactate production in a human brain infarct by infusing a stable stroke patient with [1-^{13}C]glucose and observing the ^{13}C isotopic turnover of the stroke-increased lactate pool (61).

MRS Methods for Measuring Glucose Transport and Metabolism. The concentration of glucose, the primary brain fuel, has been measured in the human brain by ^1H (62–64) and by ^{13}C (65) MRS. ^{13}C MRS measurements were used to evaluate the kinetic parameters of glucose transport across the blood–brain barrier in a 144-cm^3 volume of occipital cortex. In the ^{13}C MRS experiments, the brain glucose concentration (G_i) was measured at different concentrations of plasma glucose (G_o) under steady-state conditions (65). The data were then fitted to the accepted symmetrical Michaelis–Menten model of glucose transport across the blood–brain barrier:

$$\frac{dG_i}{dt} = \frac{G_o}{G_o + K_t} T_{max} - \frac{G_i}{G_i + K_t} T_{max} - CMR_{glc}, \quad [3]$$

in which the change in brain glucose with time, dG_i/dt, was set equal to zero to determine the transport parameters T_{max} and K_t. With the regional glucose metabolic rate ($rCMR_{glc}$) assumed to be 0.3 mM/min, based on previous measurements by PET (66), a value of 1.08 mM/min was determined for T_{max} and 4.9 ± 0.9 mM for K_t. Recently we have demonstrated that similar glucose transport kinetic parameters can be determined by using ^1H NMR (67) during a transient measurement after plasma glucose is rapidly increased. The ^1H MRS measurements have a potential volume resolution of <12 cm^3.

MRS Methods for Measuring the Tricarboxylic Acid Cycle Rate (V_{tca}). To study cerebral glucose metabolism by MRS, methods have been developed to follow ^{13}C label from enriched [1-^{13}C]glucose as it is metabolized. The most sensitive experiment consists of infusing enriched [1-^{13}C]glucose into a vein and measuring the turnover rate of the ^{13}C isotope in the brain glutamate pool. To improve sensitivity, the ^{13}C enrichment of the C4 position of glutamate is measured by observing its effect upon the proton resonance of the geminal protons (68). Animal studies using this method (68, 69) have been interpreted to give quantitative values of V_{tca} by fitting the measurements to a model validated in the rat brain (70). The tricarboxylic acid cycle flux can be directly compared with $rCMRO_2$ by using established stoichiometric relationships. A study by Rothman *et al.* (71) measured the time course of ^{13}C-label incorporation into C4 of glutamate in 24 cm^3 of human occipital cortex at 2.1 T and found good agreement with reported PET measurements of $rCMRO_2$ and $rCMR_{glc}$. Recent improvements in the MRS methodology at 2.1 T allow determination of V_{tca} in $\approx$6 cm^3 of the cortex with a statistical accuracy based on measurement noise of $\pm$7% (72). With optimized electronics at a field of 4 T, a further 2- to 4-fold spatial resolution improvement should be achievable.

MRS Studies of Visual Stimulation. PET studies of the visual cortex published in 1988 (73) reported that upon stimulation with a moving checkerboard pattern, the value of $rCMR_{glc}$ increased by $\approx$50%, while $rCMRO_2$ increased only $\approx$5%. Regional cerebral blood flow also increased by $\approx$50% during visual stimu-

lation. The decoupling between glucose and oxygen metabolic rates led to the suggestion that anaerobic glycolysis supplied the additional cerebral energy needs during visual stimulation, in which case lactate should be formed. An earlier study of stimulation of the rat paw had shown an increase of CMR_{glc} and lactate concentration in the somatosensory cortex, and anaerobic glycolysis was suggested to be the energy source (74).

To test the reported increase in anaerobic glycolysis during visual stimulation, Prichard *et al.* (75) performed ^1H NMR measurements of human visual cortex during visual stimulation and found an ≈50% (0.3 mM) increase in lactate, which peaked within 6 min after the start of the stimulus. To obtain adequate sensitivity, the spectra were acquired in 6-min periods in ≈12 cm^3 centered in the visual cortex. A subsequent study by Sappey-Marinier *et al.* (76) confirmed this increase in lactate level during visual stimulation and found a similar peak lactate increase within 6 min. Using inter- and intrasubject averaging to obtain 3-min time resolution, Jenkins *et al.* (77) found that the peak lactate increase occurs within 3 min after the start of stimulation. The appearance of lactate is consistent with the proposed increase in anaerobic glycolysis, but the change was smaller than expected from the ≈50% increase of CMR_{glc} reported by PET if this increase were sustained for the 40 min required for the $rCMR_{glc}$ measurements. A possible explanation for this discrepancy is that the mismatch between $rCMRO_2$ and $rCMR_{glc}$ is transient, which is not in contradiction to the PET data (73) because $rCMRO_2$ was measured within 5 min after the start of stimulation. Alternatively, the small increase observed in lactate concentration may represent a new steady state of lactate concentration because of the increased synthesis rate being balanced by an increased rate of clearance. These possibilities are presently being investigated by MRS and MRI studies. Analogous observations of lactate increase have been measured by ^1H MRS during auditory stimulation (78).

The 50% increase of $rCMR_{glc}$ reported in PET studies during visual stimulation should decrease the glucose concentration in the visual cortex from a basal value of 1.2 mM to 0.4 mM if the kinetic parameters determined by Gruetter *et al.* (65) and Eq. 3 are applicable under activated conditions. A preliminary report by Merboldt *et al.* (79) of brain ^1H MRS measurements during visual stimulation, while not observing lactate in the resting or activated state, did report a decrease in intracerebral glucose levels in the visual cortex of ≈50%. If substantiated, this kind of measurement would provide a continuous monitor of $rCMR_{glc}$ during activation. In conjunction with MRS measurements of V_{tca}, which provides a measure of $rCMRO_2$, the time course of the mismatch observed by PET between $rCMR_{glc}$ and $rCMRO_2$ may be tested.

In summary, MRS methods now exist for measuring anaerobic glycolysis, for determining kinetics and rates of glucose transport across the blood–brain barrier, and for deriving from the glutamate turnover the tricarboxylic acid cycle flux. In addition, there is the possibility of measuring $rCMR_{glc}$ from changes in brain glucose concentration when the kinetic parameters of glucose transport remain constant. All of these MRS measurements can be made in several cm^3 of brain, with the expectation of extending this spatial resolution to ≈1 cm^3 with the higher magnetic fields becoming available for human studies.

Comparison with PET Functional Activation Measurements

PET has set the standard for noninvasive measures of $rCMR_{glc}$, $rCMRO_2$, rCBV, and rCBF. Although it is premature to compare all of the emerging NMR techniques quantitatively with these well-established PET methods, some preliminary comparisons can be made.

Functional MRI using Gd-type contrast agents has been demonstrated to measure rCBV with considerably improved spatial resolution over PET measurements and to quantitatively agree with the PET rCBV values (16–19). In functional MRI using Hb-based contrast, the activation-related signal changes depend upon rCBF, rCBV, and $rCMRO_2$ in a way that is not understood at present quantitatively. However, the ability to measure localized human brain responses to stimuli by this method has already shown 1 order of magnitude spatial-resolution improvement over $H_2^{15}O$ measurements of rCBF. This method has localized cerebral responses to visual stimulation to 1.3 × 2 × 12 mm voxels in the gray matter of the visual cortex of a single individual in a single test (38). A study of frontal cortex response to word generation (26) has obtained better spatial resolution in individual subjects (4.5 × 6 mm) than obtained in a similar PET study that required averaging of the response in 17 different subjects to demonstrate the activation (80). In addition, time resolution of <2 s for following responses to visual and motor stimuli has been obtained, and there is no limit to the number of times the measurement can be repeated because no radioactive tracers are injected. A further advantage of the MRI methods is the direct superimposability of the functional image onto a high-resolution anatomical MRI scan without the complex coregistration methods required with PET functional images.

MRS methods for measuring V_{tca} from the ^{13}C turnover of glutamate provide a similar spatial resolution to the PET $CMRO_2$ measurement and has the advantages of using the nonradioactive ^{13}C isotope and of being insensitive to activity-related changes in rCBF. MRS measurements of $rCMR_{glc}$, through brain glucose levels, promise resolution and sensitivity comparable to PET measurements of fluorodeoxyglucose uptake and have the potential advantages of measuring the metabolism of glucose rather than of a nonmetabolizable analog, of having <15-min time resolution, and of allowing continuous monitoring of $rCMR_{glc}$.

Future Developments in Functional MRI/MRS

It is clear that both MR and PET will continue in parallel to explore parameters of brain function. MRI methods for measuring functional related brain activity have already demonstrated substantial spatial and temporal resolution improvements over PET methods. The noninvasive aspect of MR measurements combined with further readily achievable improvements in MR methods may ultimately confer an advantage to this methodology for activation and glucose utilization studies. However, radioisotope methods such as PET and single-photon emission tomography (SPECT) will continue as the primary method for *in vivo* receptor binding studies.

Brain activation studies will likely develop along two related paths—clinical use and basic neuroscience research. Functional imaging promises to allow noninvasive mapping of sensory and motor cortices as well as regions involved in the receptive and expressive aspects of language prior to excisional neurosurgery. Thus, this technique may supplant the invasive electrical stimulation mapping studies now used for this purpose. Invasive preoperative diagnostic tests such as the sodium amytal, or Wada, test used to determine language laterality might be complemented or even replaced by this new technology. If different brain structures can be functionally activated by particular cognitive tasks, then it might be possible to assess the functional integrity of those structures in patients with disease. For example, if the hippocampi can be activated by a memory task, then a sclerotic hippocampus that is the site of origin of a seizure disorder might be identified by a diminished activation response to that task. Fast NMR imaging may well have the temporal resolution to track the spread of an epileptic seizure. Functional imaging may also provide a new set of dependent variables upon which the efficacy of new treat-

ments might be tested. For example, drugs designed to slow or halt the progression of a dementia or other mental disorder might be tested by longitudinal assessment of the functional integrity of an at-risk brain structure (such as the hippocampus or prefrontal cortex).

Functional imaging will complement existing methods for investigating the functional role of different brain regions. As techniques such as EPI have good temporal resolution, it might be possible to break experimental tasks into their constituent elements to better understand the role of particular brain structures in complex behaviors that involve the interaction of many brain regions. For example, activation during encoding and retrieval phases of a memory task can be observed independently at different brain sites. If the extremely high temporal resolution afforded by EPI can be realized and combined with the high spatial resolution of MR methods, then a truly dynamic picture of brain processing will be achieved in which interactions between regions on the millisecond time scale can be studied.

This work was supported by National Institutes of Health Grant (National Institute of Diabetes and Digestive and Kidney Diseases) P01-DK34576.

1. Kety, S. S. & Schmidt, C. F. (1945) *Am. J. Physiol.* **143,** 53–66.
2. Raichle, M. E. (1987) in *Handbook of Physiology: The Nervous System*, ed. Plum, F. (Am. Physiol. Soc., Bethesda, MD), Vol. 5, pp. 643–675.
3. Fox, P. T. & Raichle, M. E. (1986) *Proc. Natl. Acad. Sci. USA* **83,** 1140–1144.
4. Weinberger, D. R., Berman, K. F. & Zec, R. F. (1986) *Arch. Gen. Psychiatry* **43,** 114–125.
5. Petersen, S. E., Fox, P. T., Snyder, A. Z. & Raichle, M. E. (1990) *Science* **249,** 1041–1044.
6. Goldman-Rakic, P. S. (1987) in *Handbook of Physiology: The Nervous System*, ed. Plum, F. (Am. Physiol. Soc., Bethesda, MD), Sect. 1, Vol. 5, pp. 373–417.
7. Lauterbur, P. C. (1973) *Nature (London)* **242,** 190–191.
8. Damadian, R., Goldsmith, M. & Minkoff, L. (1977) *Physiol. Chem. Phys.* **9,** 97.
9. Moon, R. B. & Richards, J. H. (1973) *J. Biol. Chem.* **248,** 7246–7278.
10. Radda, G. K., Bore, P. J. & Rajagopala, B. (1984) *Br. Med. Bull.* **40,** 155–159.
11. Prichard, J. W. & Shulman, R. G. (1986) *Annu. Rev. Neurosci.* **9,** 61–85.
12. Haase, A., Frahm, J., Matthaei, D., Hanicke, W. & Merboldt, K. D. (1986) *J. Magn. Reson.* **67,** 258–266.
13. Mansfield, P. (1977) *J. Phys. C* **10,** L55–L58.
14. Utz, J. A., Herkens, R. J., Johnson, C. D., Shimakawa, A., Pelc, N., Glover, G., Johnson, G. A. & Spritzer, C. E. (1987) *Am. J. Roentgenol.* **148,** 629–633.
15. Frahm, J., Merboldt, K. D., Bruhn, H., Gyngell, M. L., Hanicke, W. & Chien, D. (1990) *Magn. Reson. Med.* **13,** 150–157.
16. Belliveau, J. W., Kennedy, D. N., McKinstry, R. C., Buchbinder, B. R., Weisskoff, R. M., Cohen, M. S., Vevea, J. M., Brady, T. J. & Rosen, B. R. (1991) *Science* **254,** 716–719.
17. Villringer, A., Rosen, B. R., Belliveau, J. W., Ackerman, J. L., Lauffer, R. B., Buxton, R. B., Chao, Y.-S., Wedeen, V. J. & Brady, T. J. (1988) *Magn. Reson. Med.* **6,** 164–174.
18. Rosen, B. R., Belliveau, J. W., Vevea, J. M. & Brady, T. J. (1990) *Magn. Reson. Med.* **14,** 249–265.
19. Belliveau, J. W., Rosen, B. R., Kantor, H. L., Rzedzian, R. R., Kennedy, D. N., McKinstry, R. C., Vevea, J. M., Cohen, M. S., Pykett, I. L. & Brady, T. J. (1990) *Magn. Reson. Med.* **14,** 538–546.
20. Ogawa, S., Lee, T. M., Nayak, A. S. & Glynn, P. (1990) *Magn. Reson. Med.* **14,** 68–78.
21. Ogawa, S., Lee, T. M., Kay, A. R. & Tank, D. W. (1990) *Proc. Natl. Acad. Sci. USA* **87,** 9868–9872.
22. Turner, R., Le Bihan, D., Moonen, C. T. W., Despres, D. & Frank, J. (1991) *Magn. Reson. Med.* **22,** 159–166.
23. Bandettini, P. A., Wong, E. C., Hinks, R. S., Tikofsky, R. S. & Hyde, J. S. (1992) *Magn. Reson. Med.* **25,** 390–397.
24. Kwong, K. K., Belliveau, J. W., Chesler, D. A., Goldberg, I. A., Weisskoff, R. M., Poncelet, B. P., Kennedy, D. N., Hoppel, B. E., Cohen, M. S., Turner, R., Cheng, H.-M., Brady, T. J. & Rosen, B. R. (1992) *Proc. Natl. Acad. Sci. USA* **89,** 5675–5679.
25. Ogawa, S., Tank, D. W., Menon, R., Ellermann, J., Kim, S.-G., Merkle, H. & Ugurbil, K. (1992) *Proc. Natl. Acad. Sci. USA* **89,** 5951–5955.
26. Blamire, A., Ogawa, S., Ugurbil, K., Rothman, D., McCarthy, G., Ellerman, J., Hyder, F., Rattner, Z. & Shulman, R. (1992) *Proc. Natl. Acad. Sci. USA* **89,** 11069–11073.
27. DeVoe, E. A., Neitz, J., Bandettini, P. A., Wong, W. C. & Hyde, J. S. (1992) *Soc. Magn. Res. Med. Abstr.* **11,** 1824.
28. Fox, P. T. & Raichle, M. E. (1985) *Ann. Neurol.* **17,** 303–305.
29. Turner, R., Jezzard, P., Wen, H., Kwong, K., Le Bihan, P. & Balaban, R. (1992) *Soc. Magn. Reson. Med. Abstr.* **11,** 304.
30. Hajnal, J. V., White, S. J., Pennock, J. M., Oatridge, A., Baudovin, C. J., Young, I. R. & Bydder, G. M. (1992) *Soc. Magn. Reson. Med. Abstr.* **11,** 1023.
31. Frahm, J., Bruhn, H., Merboldt, H. D. & Haniche, W. (1992) *Soc. Magn. Reson. Med. Abstr.* **11,** 1820.
32. Bandettini, P. A., Wong, E. C., Hinks, R. S., Tihofsky, P. S. & Hyde, J. S. (1992) *Soc. Magn. Reson. Med. Abstr.* **11,** 302.
33. Kim, S.-G., Merkle, M., Ashe, J., Georgopoulos, A., Menon, R., Ellermann, J., Ogawa, S., Tank, D. & Ugurbil, K. (1992) *Soc. Magn. Reson. Med. Abstr.* **11,** 1825.
34. Sanders, J., George, J., Levine, J., Caprihan, A. & Belliveau, J. (1992) *Soc. Magn. Reson. Med. Abstr.* **11,** 1819.
35. Gore, J. C., McCarthy, G., Constable, R. T., Anderson, A. W., Kennan, R. P., Rattner, Z. & Zhong, J. (1992) *Soc. Magn. Reson. Med. Abstr.* **11,** 1826.
36. Belliveau, J. W., Kwong, K. K., Baker, J. R., Stern, C. E., Benson, R., Goldberg, I. E., Cohen, M. S., Kennedy, D. N., Brady, T. J. & Rosen, B. R. (1992) *Soc. Magn. Reson. Med. Abstr.* **11,** 310.
37. LeBihan, D., Turner, R., Jezzard, P., Cuenod, C. A. & Zeffiro, T. (1992) *Soc. Magn. Reson. Med. Abstr.* **11,** 311.
38. Menon, R. S., Ogawa, S., Kim, S.-G., Merkle, H., Tank, D. W. & Ugurbil, K. (1992) *Soc. Magn. Reson. Med. Abstr.* **11,** 309.
39. Bandettini, P. A., Wong, E. C., Hinks, R. S., Estkowski, L. & Hyde, J. S. (1992) *Soc. Magn. Reson. Med. Abstr.* **11,** 719.
40. Baker, J. R., Cohen, M. S., Stern, C. E., Kwong, K. K., Belliveau, J. W. & Rosen, B. R. (1992) *Soc. Magn. Reson. Med. Abstr.* **11,** 1822.
41. Blamire, A. M., McCarthy, G., Gruetter, R., Rothman, D. L., Ratter, Z., Hyder, F. & Shulman, R. G. (1992) *Soc. Magn. Reson. Med. Abstr.* **11,** 1834.
42. Rao, S. M., Bandettini, P. A., Wong, E. C., Yetkin, F. Z., Hammeke, T. A., Mueller, W. M., Goldman, R. S., Morris, G. L., Antuono, P. G., Estkowski, L. D., Haughton, V. M. & Hyde, J. S. (1992) *Soc. Magn. Reson. Med. Abstr.* **11,** 1827.
43. Kety, S. S. (1951) *Pharmacol. Rev.* **3,** 1–41.
44. Ackerman, J. J. H., Coleen, S. E., Becker, N. N. & Shalwitz, R. A. (1987) *Proc. Natl. Acad. Sci. USA* **84,** 4099–4102.
45. St. Lawrence, K. S., Lee, T.-Y., Yeung, W. T. I. & Henderson, S. (1992) *Soc. Magn. Reson. Med. Abstr.* **11,** 716.
46. Furuya, Y., Ikehira, H., Fukuda, N., Yamada, K., Hashimoto, T., Tateno, Y., Ueshima, Y., Yamamoto, T. & Nakajima, S. (1992) *Soc. Magn. Reson. Med. Abstr.* **11,** 1005.
47. Ewing, J. W., Jiang, Q., Chen, Q., Butt, S. M., Zhang, Z. G. & Chopp, M. (1992) *Soc. Magn. Reson. Med. Abstr.* **11,** 1105.
48. Kwong, K. K., Hopkins, A. L., Belliveau, J. W., Chesler, D. A., Porkka, L. M., McKinstry, R. C., Finelli, D. A., Hunter, G. J., Moore, J. B., Barr, R. G. & Rosen, B. R. (1991) *Magn. Reson. Med.* **22,** 154–158.
49. Hopkins, A. L., Finelli, D. A., Bhatti, S. V. & Lust, W. D. (1992) *Soc. Magn. Reson. Med. Abstr.* **11,** 1833.
50. Williams, D. S., Detre, J. A., Leigh, J. S. & Koretsky, A. P. (1992) *Proc. Natl. Acad. Sci. USA* **89,** 212–216.
51. Roberts, D. A., Detre, J. A., Insko, E. K., Bolinger, L. & Leigh, J. S. (1992) *Soc. Magn. Reson. Med. Abstr.* **11,** 305.
52. Gruetter, R. & Boesch, C. (1992) *J. Magn. Reson.* **96,** 323–334.
53. Behar, K. L., den Hollander, J. A., Stromski, M. E., Ogino, T., Shulman, R. G., Petroff, O. A. C. & Prichard, J. W. (1983) *Proc. Natl. Acad. Sci. USA* **80,** 4945–4948.

54. Rothman, D. L., Behar, K. L., Hetherington, H. P. & Shulman, R. G. (1984) *Proc. Natl. Acad. Sci. USA* **81,** 6330–6334.
55. Bottomley, P. A., Edelstein, W. A., Foster, T. H. & Adams, W. A. (1985) *Proc. Natl. Acad. Sci. USA* **82,** 2148–2152.
56. Luyten, P. R., Marien, A. J. H., Sijtsma, B. & den Hollander, J. A. (1986) *J. Magn. Reson.* **67,** 148–155.
57. Hanstock, C. C., Rothman, D. L., Prichard, J. W., Jue, T. & Shulman, R. G. (1988) *Proc. Natl. Acad. Sci. USA* **85,** 1821–1825.
58. Berkelbach van der Sprenkel, J. W., Luyten, P. R., van Rijen, P. C., Tulleken, C. A. F. & den Hollander, J. A. (1988) *Stroke* **19,** 1556–1560.
59. Bruhn, H., Frahm, J., Gyngell, M. L., Merkboldt, K. D., Hanicke, W. & Sauter, R. (1989) *Magn. Reson. Med.* **9,** 126–131.
60. Graham, G. D., Blamire, A. M., Howseman, A. M., Rothman, D. L., Fayad, P. B., Brass, L. M., Petroff, O. A. C., Shulman, R. G. & Prichard, J. W. (1992) *Stroke* **23,** 333–340.
61. Rothman, D. L., Howseman, A. M., Graham, G. D., Petroff, O. A. C., Lantos, G., Fayad, P. B., Brass, L. M., Shulman, G. I., Shulman, R. G. & Prichard, J. W. (1991) *Magn. Reson. Med.* **21,** 302–307.
62. Michaelis, T., Merboldt, K. D., Hanicke, W., Gyngell, M. L. & Frahm, J. (1991) *NMR Biomed.* **5,** 90.
63. Kreis, R. & Ross, B. D. (1991) *Soc. Magn. Reson. Med. Abstr.* **10,** 401.
64. Gruetter, R., Rothman, D. L., Novotny, E. J., Shulman, G. I., Prichard, J. W. & Shulman, R. G. (1992) *Magn. Reson. Med.* **27,** 183–188.
65. Gruetter, R., Novotny, E. J., Boulware, S. D., Rothman, D. L., Mason, G. F., Shulman, G. I., Shulman, R. G. & Tamborlane, W. V. (1992) *Proc. Natl. Acad. Sci. USA* **89,** 1109–1112, and erratum (1992) **89,** 12208.
66. Heiss, W. D., Pawlik, G., Herholz, K., Wagner, R., Goldner, H. & Wienhard, K. (1984) *J. Cereb. Blood Flow Metab.* **4,** 212–223.
67. Novotny, E. J., Gruetter, R., Rothman, D. L., Boulware, S. D. & Shulman, R. G. (1992) *Soc. Magn. Reson. Med. Abstr.* **11,** 1961.
68. Rothman, D. L., Behar, K. L., Hetherington, H. P., den Hollander, J. A., Bendall, M. R., Petroff, O. A. C. & Shulman, R. G. (1985) *Proc. Natl. Acad. Sci. USA* **82,** 1633–1637.
69. Fitzpatrick, S. M., Hetherington, H. P., Behar, K. L. & Shulman, R. G. (1990) *J. Cereb. Blood Flow Metab.* **10,** 170–179.
70. Mason, G. F., Rothman, D. L., Behar, K. L. & Shulman, R. G. (1992) *J. Cereb. Blood Flow Metab.* **12,** 434–447.
71. Rothman, D. L., Novotny, E. J., Shulman, G. I., Howseman, A. M., Petroff, O. A. C., Mason, G. F., Nixon, T., Hanstock, C. C., Prichard, J. W. & Shulman, R. G. (1992) *Proc. Natl. Acad. Sci. USA* **89,** 9603–9606.
72. Chen, W., Rothman, D. L. & Shulman, R. G. (1992) *Soc. Magn. Reson. Med. Abstr.* **11,** 3833.
73. Fox, P. T., Raichle, M. E., Mintun, M. A. & Dence, C. (1988) *Science* **241,** 462–464.
74. Ueki, M., Linn, F. & Hossman, K. A. (1988) *J. Cereb. Blood Flow Metab.* **8,** 486–494.
75. Prichard, J., Rothman, D., Novotny, E., Petroff, O., Kuwabara, T., Avison, M., Howseman, A., Hanstock, C. & Shulman, R. (1991) *Proc. Natl. Acad. Sci. USA* **88,** 5829–5831.
76. Sappey-Marinier, D., Calabrese, G., Fein, G., Hugg, J. W., Biggins, C. & Weiner, M. W. (1992) *J. Cereb. Blood Flow Metab.* **12,** 584–592.
77. Jenkins, B. G., Belliveau, J. W. & Rosen, B. R. (1992) *Soc. Magn. Reson. Med. Abstr.* **11,** 2145.
78. Singh, M., Kim, H., Huang, H. & Kim, T. (1992) *Soc. Magn. Reson. Med. Abstr.* **11,** 2146.
79. Merboldt, K.-D., Bruhn, H., Hanicke, W., Michaelis, T. & Frahm, J. (1992) *Magn. Reson. Med.* **25,** 187–194.
80. Petersen, S. E., Fox, P. T., Posner, M. I., Mintun, M. & Raichle, M. E. (1988) *Nature (London)* **331,** 585–589.
81. Turner, R., Jezzard, P., Wen, H., Kwong, K. K., Le Bihan, D., Zeffiro, T. & Balaban, R. S. (1993) *Magn. Reson. Med.* **29,** 277–279.
82. Kim, S.-G., Ashe, J., Georgopoulos, A. P., Merkle, H., Ellermann, J., Menon, R. S., Ogawa, S. & Ugurbil, K. (1993) *J. Neurophys.* **69,** 297–302.